Journal of Sol-Gel Science and Technology
https://doi.org/10.1007/s10971-025-06668-x

ORIGINAL PAPER

# Synthesize and characterization of a novel sol–gel-driven $Bi_2O_3$ semiconductor: complete degradation and fast photocatalytic activity for paracetamol

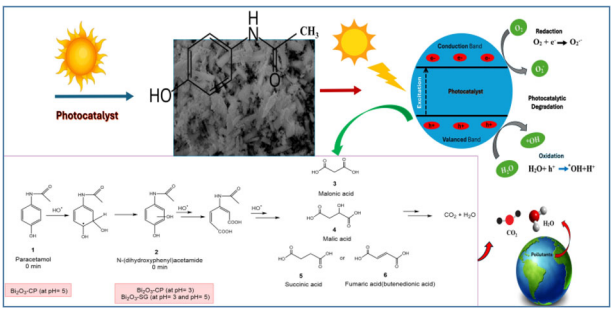
Derman Akşit[1] · Cigdem Sayil[2] · Gülin Selda Pozan Soylu[1]

Received: 4 October 2024 / Accepted: 7 January 2025
© The Author(s) 2025

## Abstract

The pollutants are getting released fluently as a waste from the pharmaceutical pollutants leading to the decrease in quality of water. The widespread occurrence of pharmaceutical pollutants poses a serious threat to the environment and human health. Besides, today carbon dioxide emissions and other forms of pollution appear to be a critical global issue. In this study, $Bi_2O_3$ catalyst has been prepared via co-precipitation (CP) and a facile sol–gel (SG) methods used as photocatalyst for the degradation of paracetamol (PAR) under different light sources. The preparation method has significant effect on the optical and structural properties of the catalysts. The tetragonal phase of $Bi_2O_3$, the presence of more surface OH groups and lower band gap energy remarkably improved the sun-light-driven photoactivity of PAR. The photocatalysts have been characterized by some structural and morphological analysis techniques and optical analysis techniques. In addition, zeta potential (ZP) measurements were performed to explain the impact of the initial pH of solution on photocatalytic degradation. Identification of PAR and the reaction intermediates was determined using Liquid Chromatography-Mass/Mass Spectrometry (LC-MS/MS) technique. Higher photocatalytic activity was obtained with the $Bi_2O_3$-SG (1:2) catalyst at pH 5 compared to the activity of $Bi_2O_3$-CP. Moreover, $Bi_2O_3$-SG (1:2) achieved the highest photocatalytic activity at pH 3. The photocatalytic activity was enhanced, and the time required for 100% degradation of PAR was reduced from 60 min to 30 min and 15 min under UVB irradiation and directly sun light irradiation, respectively. The highest reaction rate (0.086 ($min^{-1}$)) were obtained in 15 min with the $Bi_2O_3$-SG (1:2) catalyst. The results showed TOC removal could be achieved in 60 min 99.19 and 88.97% for $Bi_2O_3$-SG and $Bi_2O_3$-CP, respectively. In general, sol–gel-driven $Bi_2O_3$ as a flower and needle-like morphology, can reveal excellent opportunities in the photocatalytic technology.

## Graphical Abstract




**Keywords** Paracetamol · Photocatalytic degradation · $Bi_2O_3$ · Sol-gel · UV-B · Sunlight

✉ Gülin Selda Pozan Soylu
gpozan@iuc.edu.tr

[1] Department of Chemical Engineering, Faculty of Engineering, Istanbul University-Cerrahpasa, Istanbul, Türkiye

[2] Department of Chemistry, Faculty of Engineering, Istanbul University-Cerrahpasa, Istanbul, Türkiye

Published online: 25 January 2025

**Highlights**

- Sol–gel-driven $Bi_2O_3$ achieved complete paracetamol rapid degradation in a short time under sunlight.
- The preparation method significantly influenced nanoparticle morphologies and optical properties.
- The initial pH of PAR solution changed the degradation efficiency and reaction pathway.
- Enhanced photocatalytic activity due to reduced band gap energy, increased surface area, and decreased electron-hole recombination rates.
- Sol–gel-driven $Bi_2O_3$ holds potential for developing efficient and stable photocatalysts for environmental remediation.

## 1 Introduction

Water is one of the most important substances for all forms of life and very abundant on Earth. However, aquatic resources such as salted water of oceans and seas (97.2% water total mass) and glaciers (2.15%) are not directly usable by human beings. Less than 1% of the water total mass can be directly used by humans [1]. Therefore, clean and non-polluted water is absolutely indispensable for all living organisms including human beings. But currently, its availability is a big problem. In the future, because of the global industrialization and increase in population, this problem will gradually increase [2]. In addition, pharmaceutical compounds are not oxidized in the traditional treatment plants for treatment of wastewater [3]. That is why the pharmaceutical pollution has become increasingly serious causing irreversible damage to the environment [4]. The photocatalytic degradation method is preferred in the removal of pharmaceutical compounds in water [5]. Compared with other advanced oxidation process (UV-$H_2O_2$, UV-$O_3$, Fenton/Fenton-like), semiconductor photocatalysis utilizes green and sustainable solar energy, making it a promising method for efficiently removing pollutants.

In our study, we focused on paracetamol (PAR) called as acetaminophen [6–9], 4-acetamidophenol [9], N-acetyl-p-aminophenol [6] or 4′-hydroxyacetanilide [6] that is heavily used as antipyretic, analgesic [6–8, 10, 11] and anti-inflammatory [12] drug all over the world.

Semiconductor materials have a great attention in environmental purification and solar energy conversion [13].

This is due to their high rate of reactive oxygen species generation, photocatalytic activity, and quantum efficiency [14].

However, the practical applications of traditional photocatalysts are limited by their inherent defects, such as low utilization of visible light, easy recombination of photogenerated charge carrier, and photocorrosivity [15–17].

Among various types of photocatalysts, the most commonly used catalysts in water purification by photocatalytic processes are titanium dioxide ($TiO_2$) and zinc oxide (ZnO) catalysts [18]. Lum et al. [19], addition of incense ash (IA), which is produced in high amounts especially in Asian countries, onto ZnO at different rates (ZnO:IA = 1:1, 1:2, 1:3, 1:4, 1:5) They develope a new catalyst (IA supported ZnO) and used it for PAR photodegradation. It was determined that PAR degradation with IA doping increased significantly compared to pure ZnO and pure IA, and the optimal doping ratio was 1:1. In 60 min, 36% degradation efficiency was achieved with pure ZnO, 2.7% with pure IA, and 57% with ZnO/IA (1:1) nanocomposite [19].

Mohammad Shakir et al. [20], synthesized La-doped ZnO [Zn1-xLaxO ($x = 0.0$–$0.01$–$0.03$ and $0.05$)] and examined the degradation of PAR under visible light. A solution concentration of 5 ppm was prepared and 0.1 g of photocatalyst was added to 100 mL of PAR solution (pH = 9). A 300 W Xe lamp was used as the light source. It was observed that 3% La-doped ZnO photocatalyst had the highest photocatalytic activity and ~80% of the PAR was degraded in 180 min [20]. Basha et al. studied photodegradation in an aqueous system at PAR concentration in the range of 10–115 ppm using a 125 W Hg lamp in the presence of 1.5 g/L 10% IPCA $TiO_2$ catalyst. 72% PAR was removed from the 25 ppm PAR solution within 240 min [21]. Lin et al., K3[Fe(CN)6]-doped $TiO_2$ catalyst under visible light (5 blue LED lamps, $\lambda = 440$–$490$ nm, light intensity = 16.85 mW/cm$^2$) photocatalyst dosage (0.50–0.75–1.00 g/L), initial PAR concentration (0.10–0.15–0.20 mM) and initial solution pH (6.90–7, 58–8.25) carried out a series of reactions to examine and optimize effects on the photocatalytic degradation of PAR. Among the parameters examined, initial PAR concentration was found to have the most significant effect. Under optimum conditions, with an initial PAR concentration of 0.1 mM, a catalyst dosage of 1.0 g/L, and an initial solution pH of 6.94, PAR removal was determined to be 91.06% after 9 h of visible light irradiation [22].

Among many narrow band gap semiconductors, bismuth oxide ($Bi_2O_3$) is a p-type semiconductor material, is one of the most important photocatalysts due to its uniqueness structure and physical characteristics such as high refractive index, high oxygen-ion conductivity, dielectric permittivity, thermal stability [23]. It has a direct band gap of 2.85 eV for monoclinic α-$Bi_2O_3$ and 2.58 eV for tetragonal β-$Bi_2O_3$ phase, which can be excited by sunlight. It is also an important semiconductor material due to its remarkable physical properties such as high refractive index, dielectric

constant, extraordinary photoconductivity, and photoluminescence (PL). These properties have made $Bi_2O_3$ suitable for large-scale applications such as gas sensors, optical coatings, capacitors, catalysts, fuel cells, photovoltaic batteries, and microwave integrated circuits. To date, many $Bi_2O_3$ micro- and nanostructures [including nanofibers, nanoribbons, nanocables, nanoparticles, microrods, particles (sheets, templates), and thin films] have been successfully synthesized [24].

Nowadays, Bi(III)-based semiconductor materials are widely preferred in in photocatalysis. It is worth noting have a relatively narrow band gap, which belongs to band gap semiconductors, unique structural, chemical, and electrical properties can respond to visible light [25].

Natarajan et al. have synthesized Bi-doped $TiO_2$ nanotubes (Bi-TNT) photocatalyst, active under direct sunlight irradiation for decomposition of RhB dye. The photocatalytic degradation results demonstrated that RhB dye (50 mg/L) was completely degraded within 3 h using Bi-TNT photocatalyst under direct sunlight irradiation [26].

Meroni et al. prepared Bi-promoted nano-$TiO_2$ photocatalysts and final samples tested in reactions. The presence of Bi, about 30% mineralization enhancement in photocatalytic activity was achieved compared to pure $TiO_2$ [27].

BiOX (X = Br, Cl and I) nanoplate photocatalysts were synthesized and their photocatalytic activities for degradation of Rhodamine were investigated under different LEDs. 100% RhB dye degradation was achieved within 120 and 240 min under UVLED irradiation with BiOCl and BiOBr catalysts. With the BiOI catalyst, it showed 83.4% degradation under red LED (RLED) irradiation after 240 min. In this study, it was concluded that the BiOI photocatalyst could be effective in the degradation of RhB dye under cheaper RLED irradiation instead of UVLED [28].

In recent years, there have been many reports about $Bi_2MoO_6$ as a photocatalyst to remove organic pollutants driven by visible light. Dong et al. [29] developed a bilayer structure $Bi_2MoO_6$ and it degraded 94.7% of CIP in 80 min under the xenon lamp irradiation. In 2022, Liu et al. [30] designed a nanorod/nanoflake $Bi_2MoO_6$ co-junction photocatalyst with oxygen vacancies it degraded phenol by 97% in 240 min.

Briefly, $Bi_2O_3$ is an effective photocatalyst in the degradation and minerilization of hazardous compounds. However, the photocatalytic degradation reaction of paracetamol has not been observed in the presence of $Bi_2O_3$ photocatalyts.

In order to shorten these long degradation times for PAR, the nano $Bi_2O_3$ catalyst prepared by an easy and inexpensive sol–gel simple method. Besides, $Bi_2O_3$-SG catalyst was designed to investigate the effect of synthesis condition (molar ratio of bismuth acetate to oxalic acid) on photocatalytic degradation of PAR, and then the catalyst with the high photocatalytic activity was compared with $Bi_2O_3$-CP under different pH conditions, light sources. Photocatalysts were characterized using structural, optical, size and surface charge characterization techniques (XRD, BET, SEM, UV-VIS DRS, PL, and ZP and particle size distribution). After that, at least as important as the others, is to identify the degradation intermediates of PAR by LC-MS/MS technique and propose the possible pathways for PAR degradation.

## 2 Experimental

### 2.1 Materials

Bismuth(III) nitrate pentahydrate ($Bi(NO_3)_3.5H_2O$,98%) and bismuth(III) acetate ($Bi(CH_3COO)_3$, 99%) were purchased from Alfa-Aesar, and used as the Bi precursors for synthesis via CP and SG methods, respectively. Paracetamol was micronized and purchased from Sigma Aldrich. All the other solvents and reagents used in this study were purchased from Merck.

### 2.2 Preparation of $Bi_2O_3$ nanoparticles

$Bi_2O_3$ nanoparticles have been synthesized according to the following procedures.

#### 2.2.1 $Bi_2O_3$ synthesis by co-precipitation method

$Bi_2O_3$ photocatalyst was prepared using a facile co-precipitation method. $Bi(NO_3)_3.5H_2O$ and NaOH were separately dissolved in $HNO_3$ (65%) solution and deionized water, respectively. The obtained solutions were mixed magnetically for 15 min at room temperature. Hereinafter, the solution of pH value was adjusted to 11 by the addition of 0.2 M NaOH. After reaching desired pH, solution was heated and magnetically stirred at 75 °C for 2 h (the color became yellowish). After filtration, the sample was washed with water and then with absolute ethanol and dried at 80 °C for 2 h. Dried powders were calcined in an air oven at 450 °C for 2 h (10 °C/min), and after that they were milled for 5 min in a ball milling (MM200). The sample was denominated as $Bi_2O_3$-CP.

#### 2.2.2 $Bi_2O_3$ synthesis by sol–gel method

$Bi(CH_3COO)_3$ and oxalic acid anhydrous ($C_2H_2O_4$) were separately dissolved and magnetically stirred in absolute ethanol at 65 °C and 45 °C, respectively. In this process, the molar ratios of bismuth acetate to oxalic acid were 1:1, 1:2, 1:3, and 1:4. $C_2H_2O_4$ solution was added drop-by-drop into bismuth acetate solution under a high stirring rate at 45 °C, and the mixture of these solutions were stirred magnetically

for 1 h. Then, pH was adjusted to 2 by HCl addition. The sol was dried at 80 °C overnight. The resulted powders were calcined in an air oven at 400 °C for 2 h (10 °C/min), and after that they were milled for 5 min in a ball milling. The obtained catalyst was denominated as $Bi_2O_3$-SG (X), where X means the molar ratio of bismuth acetate to oxalic acid ($X = 1{:}1$, 1:2, 1:3, and 1:4).

## 2.3 Catalyst characterization

### 2.3.1 Structural and morphological analysis

The structural and/or morphological properties of synthesized catalysts were characterized using XRD, BET, and SEM techniques.

XRD analysis was conducted on a Rigaku D/Max-2200 diffractometer with the CuKα ($\lambda = 1.54056$ °A) radiation. The results were taken over the range of 2θ angles from 10° to 80°at a scanning rate of 2°/min. The BET specific surface areas of the samples by nitrogen adsorption-desorption isotherm measurements at 77 K (Quantachrome Inst.). The samples were degassed at 200 °C for 2 h prior to the actual measurements. The surface morphology of the synthesized powders was characterized using a SEM equipment (FE-SEM, FEI Quanta FEG-450).

### 2.3.2 Optical properties

The optical properties and electron-hole recombination rates were studied using an UV-VIS DRS spectrometer and a PL spectrofluorometer. To determine band gap energy values, reflectance measurements of synthesized photocatalysts were carried out on a UV-VIS DRS (Ocean Optics, Flame Miniature Spectrometer) using a UV-Vis-NIR light source (DH-2000-BAL). During the measurements, PTFE was used as a diffuse reflectance standard. PL measurement was performed with an Agilent Technologies-Cary Eclipse fluorescence spectrophotometer using a xenon lamp at an excitation wavelength of 350 nm at room temperature. Measurements were made after adding ethanol to the sample and mixing it in an ultrasonic bath.

The surface OH groups of the photocatalysts were determined by Fourier transform infrared spectroscopy. The FT-IR spectrum was recorded on a Perkin Elmer Precisely Spectrum One spectrometer at ambient conditions by using KBr asdiluent. All measurements were at 4 $cm^{-1}$ resolution and 100 scans.

### 2.3.3 ZP measurements

ZP measurements of synthesized catalysts were performed using Malvern Zetasizer Nano ZS ZEN3600 equipment (Malvern Instruments Limited, Malvern, Worcestershire, UK). Ultrapure water was used as dispersant. Both of the catalysts were dispersed at 0.1 g/100 mL in water using Silent Crusher S (Heidolph Instruments, GmbH & Co. KG, Schwabach, Germany) for 90 s. Zeta potential analysis was done in disposable folded capillary cell model DTS1070 (Malvern Panalytical Inc., Malvern, Worcestershire, UK).

## 2.4 Photocatalytic experiments and activity measurements

### 2.4.1 Photocatalytic reaction

The performances of the synthesized samples were evaluated using different light sources. UVA (8 W × 8), UVB (8 W × 8), UVC (8 W × 8), Halogen Hg Lamp (T3 120 v model, 150 W, 303–518 nm), VIS (simulated sunlight irradiation, 8 W × 8), and directly sun light using as the light sources without using cut-off filters.

The spectral irradiance of the UV lamp is from 303 to 578 nm and the illumination distance is 18 cm from the target. The light intensity of UV lamp used for degradation experiments was recorded with an UV/Visible powermeter (SmartSensor-AR823). Inaddition, the reaction was placed in an open place on a sunny day under natural sunlight in June–August.

In each experiment, 100 mg of $Bi_2O_3$ photo-catalyst was dispersed in 50 mL aqueous paracetamol solution (25 mg $L^{-1}$) and magnetically mixed for 30 min in a dark condition to ensure adsorption-desorption balance. The light sources (UVA, UVB, UVC. and VIS) were illuminated from the both sides, and the distance between the light sources, the solution was guaranteed to be 10 cm, and the reactions were carried out in the LUZCHEM LZC-5 photoreactor system. On the other hand, halogen Hg lamp was illuminated from the above, and the distance between Hg lamp and the solution was 18 cm.

Besides, during photocatalytic experiments to investigate the effect of pH, PAR solutions were prepared at different pH values (pH: 3–9). 0.1 N NaOH, 0.01 N, and 0.1 N HCl solutions were used for pH arrangements.

During the illumination, 0.3 mL of degraded solution was taken out at certain times (0, 2, 15, 30, 45, 60, 90, 120 min), and filtered with a hydrophilic PTFE filter with 0.45 µm pore size.

After irradiation, the4-chlorophenol solution was filtered through a membrane filter (poresize 0.45 mm) and the filtrate was used for TOC measurement with a TOC-V, Shimadzu equipment.

Degrading efficiency of PAR was calculated by using following Eq. (1)

$$\%\,\text{Degradation} = \frac{C_o - C}{C_o} \times 100 \quad (1)$$

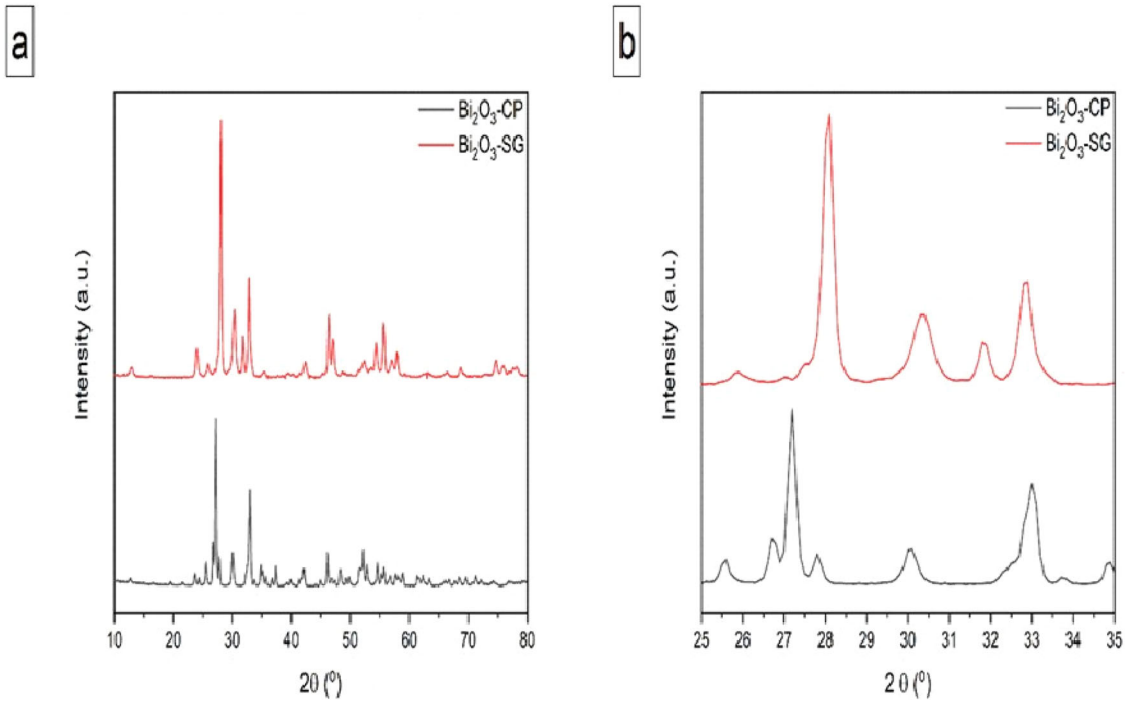



**Fig. 1** Wide (**a**) and enlarged (**b**) XRD patterns of the $Bi_2O_3$ nanoparticles synthesized with different preparation methods

Where Co, initial concentration of drug solution, Ct, concentration of drug solution at a time.

#### 2.4.2 Analytical procedure

The concentration of PAR was followed by HPLC with equipped with a C-18 column (5 µm, 150 × 4.6 mm) and the detection wavelength was selected at 242 nm. The mobile phase consisted of a mixture of acetonitrile and water with volume ratio 35:65 was filtered through hydrophilic PTFE filters (0.45 µm pore size), degassed by ultrasonication for 30 min, and the flow rate was set as 1 mL·min$^{-1}$. The temperature of the column compartment was 25 °C while the injection volume was 40 µL.

#### 2.4.3 Identification of photodegradation intermediates of PAR

PAR and the reaction intermediates were determined by LC-MS/MS system. The system was coupled with an LCMS-8040 triple quadrupole mass spectrometry (Shimadzu) and an LC-20A liquid chromatography system (Shimadzu) equipped with an Ultra-AQ C-18 column (Restek, 100 × 2.1 mm, 3 µm). Liquid chromatographic separation was established using a mobile phase consisting of 0.2% formic acid in water: methanol (MeOH) = 50:50. The column oven was set at a constant temperature of 40 °C for the duration of the analysis. The SIM (I) mode was used with Q3 scan of 100–600 m/z.

## 3 Results and discussion

### 3.1 Characterization of $Bi_2O_3$-CP and $Bi_2O_3$-SG photocatalyts

XRD analysis was conducted to identify the crystal phases, structures and crystallite size of the $Bi_2O_3$-CP and $Bi_2O_3$-SG samples. XRD diffractograms of the catalysts were shown in Fig. 1. According to the XRD patterns; peak intensity and full width at half-maximum (FWHM) data were determined. The three strongest diffraction peaks located at $2\theta = 27.2°$, 30.10° and 34.90° for $Bi_2O_3$-CP were well matched with the monoclinic crystal system of α-$Bi_2O_3$ (Cell parameters; $a = 0.58488$ nm, $b = 0.81661$ nm, $c = 0.75097$ nm) P1 21/c1 (14) space group (COD Database, entry number: 96-901-2547). On the other hand, the three strongest diffraction peaks for $Bi_2O_3$-SG catalyst with 2θ at 27.93°, 30.22° and 32.72° is belonged to tetragonal crystal system of β-$Bi_2O_3$ (Cell parameters; $a = 0.77400$ nm, $c = 0.56300$ nm) $P\bar{4}b2$ space group (117) (COD Database, entry number: 96-901-2328). Further observation indicates that the XRD peak intensity of $Bi_2O_3$-SG (β-$Bi_2O_3$) was higher than $Bi_2O_3$-CP (α-$Bi_2O_3$), which indicates that the crystallization of $Bi_2O_3$ is enhanced. The average crystallite sizes of the $Bi_2O_3$-CP and $Bi_2O_3$-SG (1:2) photocatalysts are calculated using Scherrer's equation [31] and found 41 nm and 31 nm, respectively.

In summary, that monoclinic $Bi_2O_3$-CP and tetragonal $Bi_2O_3$-SG phases of $Bi_2O_3$ were revealed in XRD analysis.

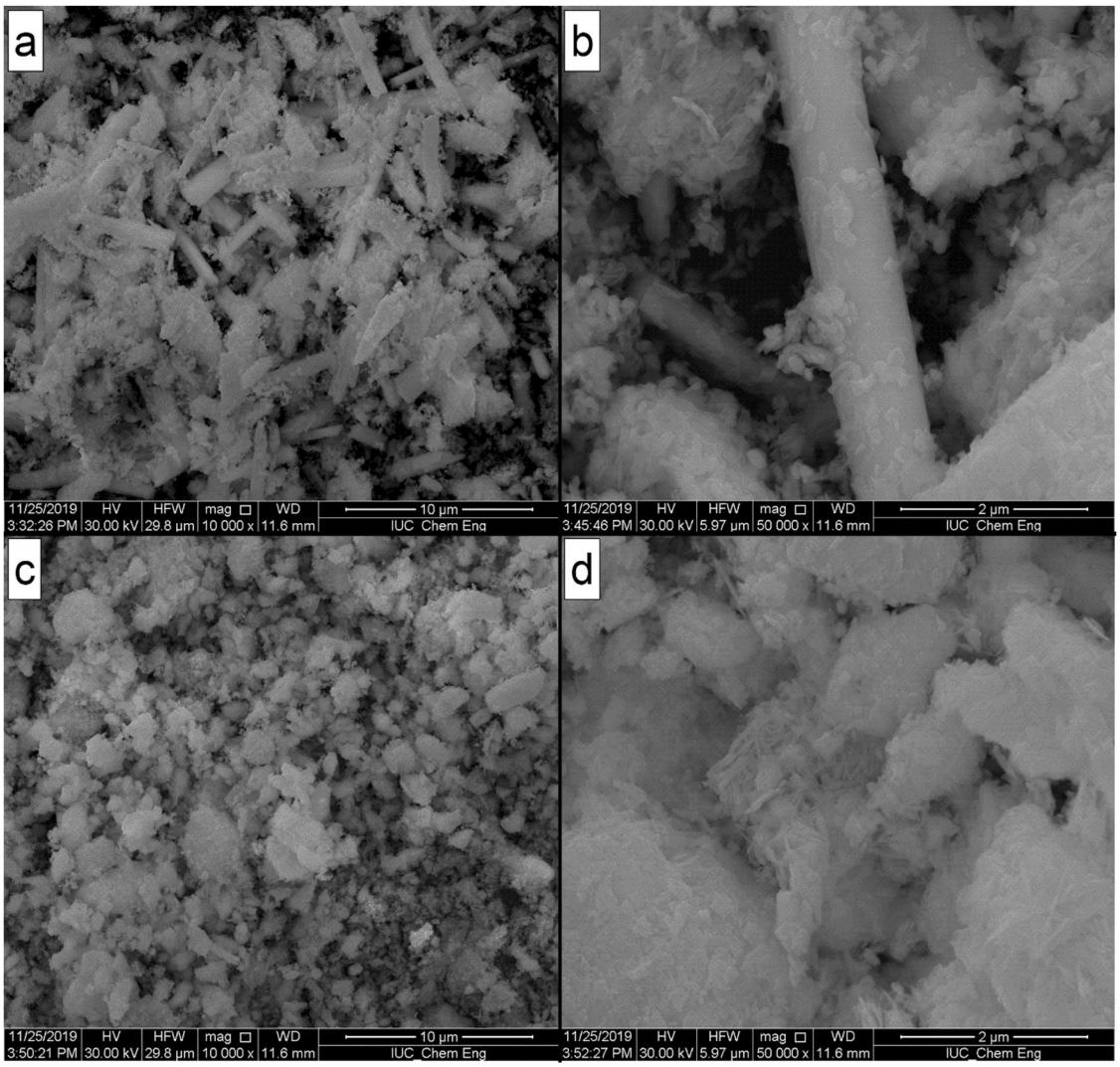



**Fig. 2** SEM images of $Bi_2O_3$-CP and $Bi_2O_3$-SG (1:2) catalysts with 10,000× (**a**), 50,000× (**b**) and 10,000× (**c**), 50,000x (**d**) magnification scales, respectively

It is clear that the photocatalytic activity is affected by the tetragonal phase.

The specific surface areas of photocatalysts were evaluated with BET technique. The specific surface area of $Bi_2O_3$-CP and $Bi_2O_3$-SG (1:2) photocatalysts were found as 12 $m^2$/g and 23 $m^2$/g, respectively; which means that the surface area of $Bi_2O_3$-SG (1:2) was about 1.8 times as large as than $Bi_2O_3$-CP. It is known that the larger specific surface area is more likely to provide closer contact between photocatalyst and contaminant allowing more active species to be absorbed on the surface of the photocatalyst during photodegradation. Moreover, the BET results are consistent with the crystallite sizes of the photocatalysts calculated using XRD data. It is seen that the crystallite size decreases and the BET specific surface area increases.

SEM images shown in Fig. 2 were used to identify the shape, morphology and size of the synthesized catalysts. Figure 2a, b represent SEM images of $Bi_2O_3$-CP which clearly indicated rod-shaped morphology with a non-uniform diameters and sizes. These nano-rods were also exhibiting a random orientation. Figure 2c, d represent SEM images of $Bi_2O_3$-SG (1:2). Macro and micro structures were found on the catalyst surface. In addition to that, heterogeneous particle structures such as flower-like and needle-like with miscellaneous dimensions were observed.

Infrared spectroscopy technology is used to detect the presence of functional groups such as hydroxyl radical (•OH) adsorbed on the surface of synthesized nanoparticles. In the photocatalytic degradation experiments, the surface OH groups can not only embrace the photogenerated holes to form hydroxyl radical (•OH) but also serve as active sites for the adsorption of reactants.

In FTIR spectra (Fig. 3), a broad band at around 3380 $cm^{-1}$ was assigned to O-H stretching mode of molecularly adsorbed

water in $Bi_2O_3$-SG [32]. $Bi_2O_3$-BC sample did not show any peaks at around 3380 $cm^{-1}$. Additionally, in the spectrum, the strong band of O-H bending arised at around 1382 $cm^{-1}$. This result indicated that the higher photocatalytic activity of $Bi_2O_3$-SG sample due to hydroxyl group in its structure. The strong absorption band at around 835 $cm^{-1}$ seemed in FTIR spectra of samples is the stretching vibration of Bi—O bonds in $BiO_6$ octahedral units [33]. The Bi—O bending vibration was observed at about 468, and 588 $cm^{-1}$ for $Bi_2O_3$-SG sample. However, these peaks observed weakly for $Bi_2O_3$-CP sample. These results indicate that $Bi_2O_3$-CP exhibits a weaker interaction under light in the reaction.

The UV-VIS DRS spectra in the percent reflectance mood for $Bi_2O_3$-CP was compared with $Bi_2O_3$-SG (1:2) in Fig. 4. In this study, the reflectance % of the samples was expressed in the 230–800 nm wavelength region. Figure 4 shows UV-Vis DR spectra of (a) $Bi_2O_3$-CP and (b) $Bi_2O_3$-SG (1:2) photo-catalysts. As seen in the Fig. 4a, $Bi_2O_3$-CP exhibits wavelength range up to ~412 nm. On the other hand, $Bi_2O_3$-SG exhibits wavelength range up to about 455 nm (Fig. 4b).

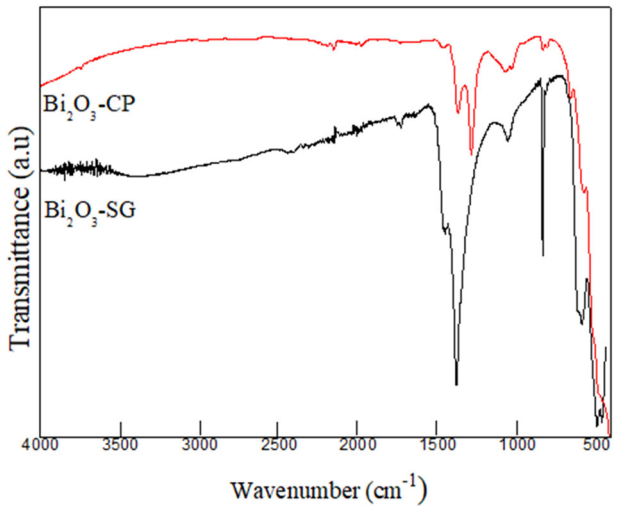



**Fig. 3** FT-IR spectrum of $Bi_2O_3$-CP and $Bi_2O_3$-SG (1:2) photocatalysts

From these spectral data, the optical band gap energies ($E_{bg}$) of resulted photo-catalysts were estimated using Kubelka-Munk equation and the Tauc plot.

Kubelka-Munk equation [34, 35] is defined by the following Eq. (2)

$$F(R) = \frac{(1-R)^2}{2R} \tag{2}$$

F(R): Kubelka-Munk function

R: Reflectance of the sample

The Tauc Plot [35, 36] is represented by the following Eq. (3)

$$[F(R) * h\nu]^{1/n} \text{vs. } h\nu \tag{3}$$

h: Planck constant ($4.135 \times 10^{-15}$ eV.s)

$\nu$: Photon's frequency

n: Sample transition constant

By extrapolated the straight line to the x-axis in Tauc plot, $E_{bg}$ values of the synthesized catalysts could be estimated. In this study, the constant n was taken as ½ and 2 by assuming the $E_{bg}$ of $Bi_2O_3$ is direct and indirect allowed transition, respectively. As shown in Fig. 5a, b, the $E_{bg}$ values of $Bi_2O_3$-CP for direct and indirect transition are calculated to be 2.97 eV and 3.18 eV, respectively. Some studies have reported that the difference between direct and indirect transition for monoclinic phase of $Bi_2O_3$ is ~0.1 eV

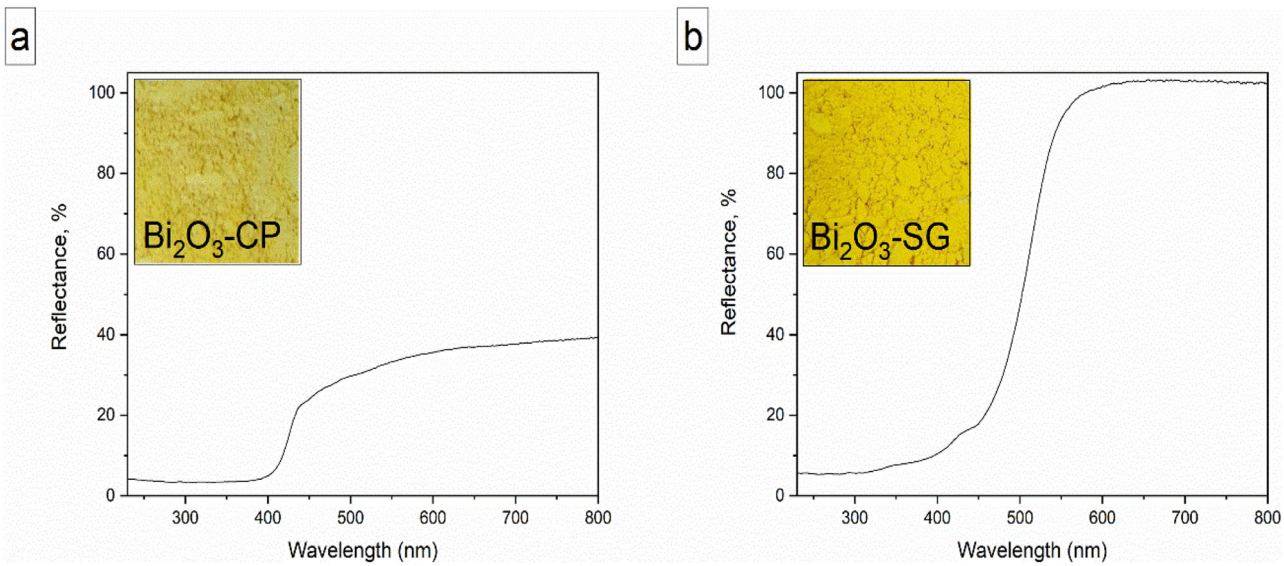



**Fig. 4** UV-Vis DRS of $Bi_2O_3$-CP (**a**) and $Bi_2O_3$-SG (1:2) (**b**) photocatalysts

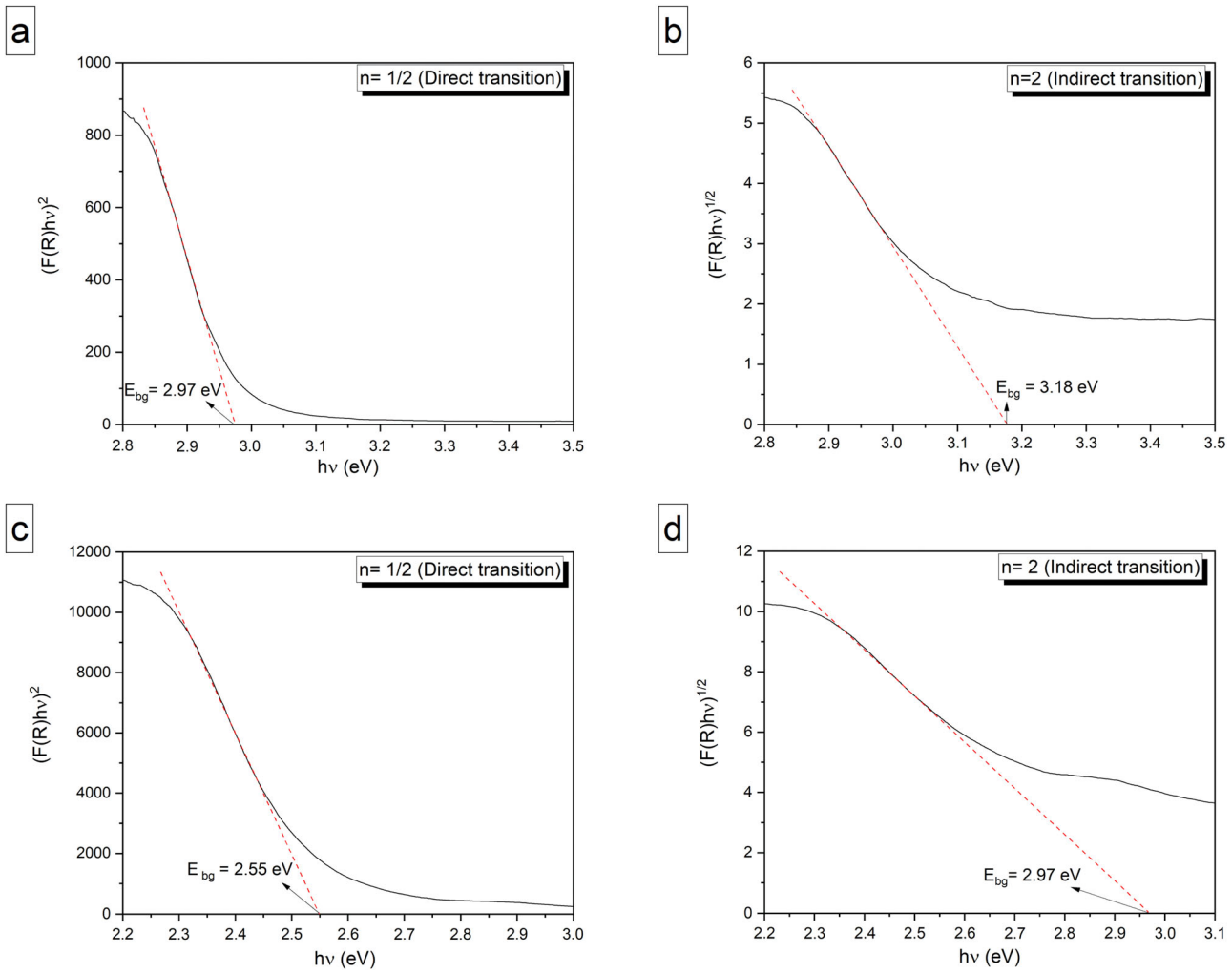



**Fig. 5** Tauc plot $[F(R)h\nu]^{n/2}$ vs. hν of $Bi_2O_3$-CP (**a**, **b**), $Bi_2O_3$-SG (1:2) (**c**, **d**) photocatalysts with the assumption of the direct ($n = ½$) and indirect ($n = 2$) allowed transition, respectively

[37–39]. However, in this study we found that is about 0.21 eV, which is significantly higher than the reported values. As seen in Fig. 5c, d, the calculated $E_{bg}$ values of $Bi_2O_3$-SG (1:2) for direct and indirect transition are 2.55 eV and 2.97 eV, respectively. A decrease in the band gap is expected due to the increase in carrier concentration [40]. As it can be clearly seen from the obtained graphs, it was determined that both $Bi_2O_3$-CP and $Bi_2O_3$-SG (1:2) catalyst were more suitable for the direct transition ($n = 1/2$) assumption.

The electron-hole recombination rates of the as-prepared $Bi_2O_3$-CP and $Bi_2O_3$-SG (1:2) photocatalysts were investigated by PL spectroscopy as shown in Fig. 6. The emission spectra were obtained at the excitation wavelength ($\lambda_{ex}$) of 350 nm. As seen in Fig. 6a, a strong red band emission was observed at 705 nm (1.76 eV) upon photoexcitation at 350 nm ($\lambda_{ex}$). No shift was observed in the wavelength at which the catalysts showed the strongest emission, but a

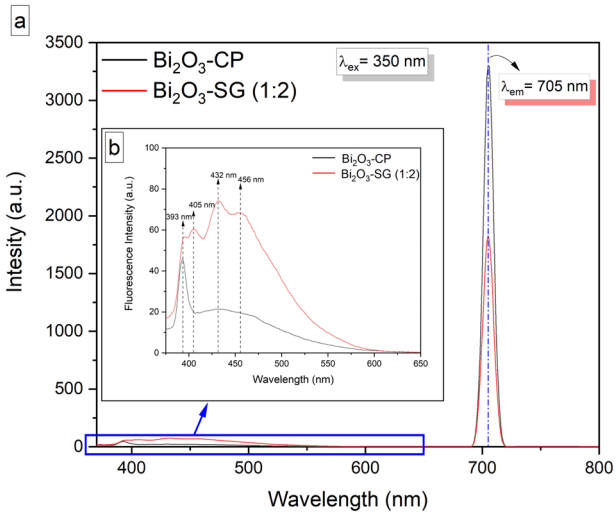



**Fig. 6** PL spectra (**a**), Enlarged-PL spectra of $Bi_2O_3$-CP and $Bi_2O_3$-SG (1:2) nanoparticles, excited at the wavelength of 350 nm (**b**)

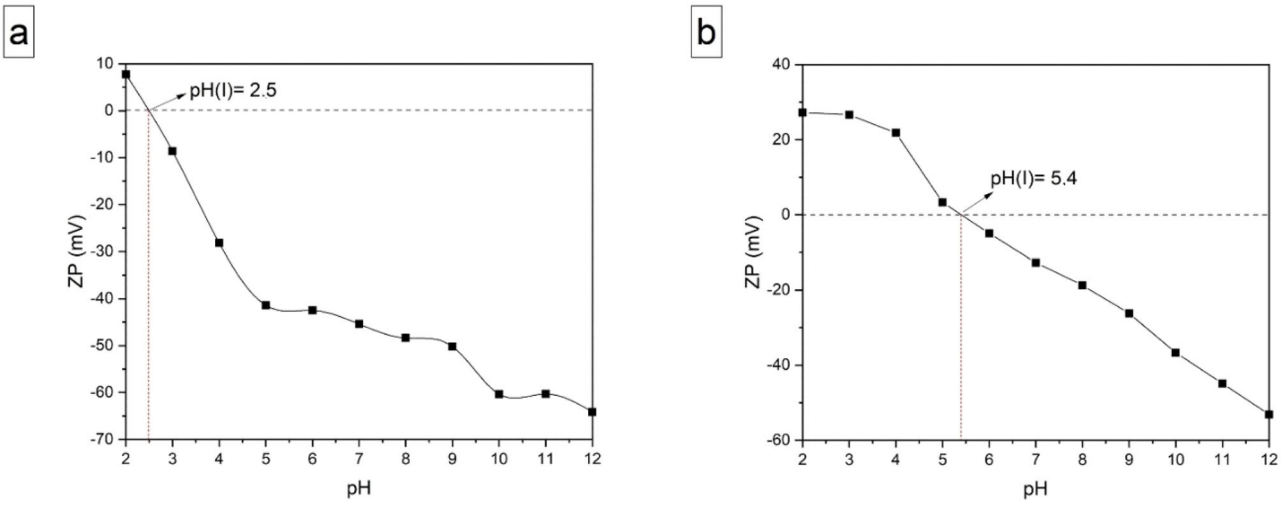



**Fig. 7** Zeta potential and pH(I) values of $Bi_2O_3$-CP (**a**) and $Bi_2O_3$-SG (1:2) (**b**) photocatalysts

significant change in emission intensities was observed. The lower PL intensity means the decrease in recombination rate, thus it results in higher photocatalytic activity. In contrast, the stronger PL intensity exhibits a faster recombination rate [41, 42]. The PL spectra of $Bi_2O_3$-SG (1:2) showed lower intensity. In addition, some studies have reported this intense red band emission observed at 705 nm. In those studies, band at 705 nm can also be associated with the level of crystal defects or crystal defects originated from the oxygen vacancy ($V_O$) or Bi interlayer ($Bi_i$) during crystal growth [43, 44]. The $Bi_2O_3$ catalysts showed a series of PL bands in the range of 380–600 nm. In Fig. 6(b), the enlarged PL spectra between 370 nm and 650 nm were shown. $Bi_2O_3$-CP had a sharp and a broad PL emission peaks centered at about 393 nm (3.16 eV) and 432 nm (2.87 eV), respectively. On the other hand, $Bi_2O_3$-SG (1:2) had four PL emission peaks centered at about 393 nm (3.16 eV), 405 nm (3.06 eV), 432 nm (2.87 eV) and 456 nm (2.72 eV). The highest emission band was centered at 393 nm for $Bi_2O_3$-CP, whereas it was centered at 432 nm for $Bi_2O_3$-SG (1:2).

It is clearly seen that different preparation ways showed different signal curve and shape. The obtained results from PL spectra are also in good agreement with the activity results.

In photocatalytic degradation reactions, pH plays an important role since it has a strong influence on the adsorption of the pollutant on the catalyst surface. In this study, to investigate surface charges of the $Bi_2O_3$ samples dispersed in aqueous suspensions, their ZP measurements were carried out in the pH range of 2–12. The pH value where ZP equals to zero which is known as isoelectric point, pH(I) [45].

The ZP measurements are shown in Fig. 7a, b. It was observed that pH(I) of $Bi_2O_3$-CP was found to be at pH 2.5 (Fig. 7a), while pH(I) of $Bi_2O_3$-SG (1:2) was found at pH 5.4 (Fig. 7b). According to some authors, at pH > pH(I), the catalyst exhibits negative surface charge and can act as an anionic exchanger. In contrast, at pH < pH (I), the surface charge of the catalyst is positive. It means that is beneficial for the adsorption of PAR anions by electrostatic attraction because of its cationic feature [45, 46].

To summarize, the optical properties of the catalyst caused difference in photocatalytic activity. It was also considered that the photocatalytic degradation of PAR could be effectively enhanced and completely removed after 60 min reaction time by UVA, UVB, UVC lights and directly sunlight irradiation using $Bi_2O_3$-SG (1:2) catalyst. In comparison, $Bi_2O_3$-CP maked the complete PAR degradation in a longer time (90 min). Additionally, 86.10 and 67.70% degradation was achieved in the case of UVC and sunlight irridation at the end of 60 min. This may be due to the difference in bandgap energy of $Bi_2O_3$-SG (1:2) and $Bi_2O_3$-CP leads to the difference in absorbing the incident photons. Moreover, the fast recombination of photoelectrons and holes when $Bi_2O_3$-CP is excited by visible light leads to the lesser degradation rate over PAR. This is credited to the very low bandgap energy of $Bi_2O_3$-CP leads to recombination of electron hole pairs which suppresses the degradation rate to some extent.

This is mainly because of $Bi_2O_3$-SG (1:2) had four PL emission peaks centered at about 393 nm (3.16 eV), 405 nm (3.06 eV), 432 nm (2.87 eV) and 456 nm (2.72 eV). Whereas, $Bi_2O_3$-CP had 393 nm (3.16 eV) and 432 nm (2.87 eV) PL emission peaks. On the otherhand, the fact that the $Bi_2O_3$-SG (1:2) catalyst has more emission peaks than the $Bi_2O_3$-CP catalyst and $Bi_2O_3$-SG (1:2) catalyst is more sensitive to light, enabled it to show activity in a wider spectrum. Ultimately, more hydroxyl radicals or holes may be produced under sunlight irradiation which leads to the degradation of PAR.

**Table 1** Degradation kinetics of PAR at pH 5 in the presence of $Bi_2O_3$-SG with different molar ratios (Bismuth acetate: Oxalic acid) under UVB irradiation

| Catalyst | Molar Ratio (Bismuth Acetate : Oxalic Acid) | Rate Constant [k ($10^{-3}$ $min^{-1}$)] | Degradation (%) (at 60 min) | Regression Coefficient ($R^2$) |
|---|---|---|---|---|
| $Bi_2O_3$-SG | 1:1 | 43.0 | 89.63 | 0.982 |
| | 1:2 | 72.5 | 100 | 0.987 |
| | 1:3 | 18.8 | 60.32 | 0.960 |
| | 1:5 | 16.6 | 56.57 | 0.955 |

## 3.2 Photocatalytic experiments and kinetic studies

The results from the photocatalytic experiments were fitted to the pseudo-first order kinetic model.

$$-\frac{d[C]}{dt} = k \tag{4}$$

$$-\ln\frac{[C]}{[C]_0} = kt \tag{5}$$

Where;

k: First order rate constant ($min^{-1}$)

$C_0$: Initial PAR concentration (ppm)

C: PAR concentration at time t

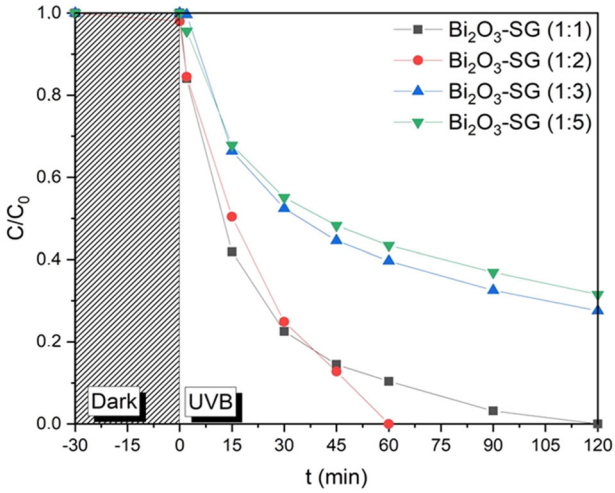



**Fig. 8** Effect of molar ratio of bismuth acetate to oxalic acid

### 3.2.1 Effect of molar ratio of bismuth acetate to oxalic acid

First of all, determination on the purpose of the photodegradation percentages of PAR with $Bi_2O_3$-SG photocatalysts synthesized using different molar ratios of bismuth acetate to oxalic acid, a series of photocatalytic reactions for 120 min were carried out under UV-B irradiation. The neutral pH of the reaction suspensions was at pH 5, and the experiments were carried out without pH adjustment. As shown in Table 1, the optimum molar ratio was found as 1:2, and it is clearly seen that all of the PAR was removed from water in 60 min using the $Bi_2O_3$-SG (1:2) photocatalyst (Fig. 8). When the molar ratio was increased from 1:1 to 1:2, the degradation rate also increased, but when the ratio was increased further, the degradation rate decreased. This result that can be drawn is that decrease in the degradation at higher molar ratio of bismuth acetate to oxalic acid can affect pores of the catalyst and surface area. The removal efficiencies are shown in Table 1.

### 3.2.2 Effect of light sources

In order to reveal the effect of light sources on the degradation of PAR, experiments were carried out keeping 25 ppm pollutant concentration, pH 5, 25 °C medium temperature. Figure 9 shows the degradation efficiency of PAR was inversely proportional to its initial concentration. In the first two experiments, the degradation of 25 ppm PAR solution was tested without any catalysts in a dark condition and under UVB irradiation. As shown in Fig. 9a, no change in the concentration was found for dark condition where as there is a decrease ~5% of the concentration within 90 min under UVB irradiation. In order to compare the activity of $Bi_2O_3$ with different morphologies a series of experiments were carried out under dark and different illumination conditions (Fig. 9b–d). As shown in Fig. 9b, removal of PAR was examined using $Bi_2O_3$-CP and $Bi_2O_3$-SG (1:2) catalysts in the dark condition. The observed PAR degradation % achieved 3.37% and 6.78% after 90 min, respectively. These reactions (Fig. 9a, b) were carried out to show that the direct photolysis and adsorption of paracetamol are negligible. In Fig. 9c, photodegradation of PAR was investigated using $Bi_2O_3$-CP catalyst by different light sources. The highest degradation % in the presence of $Bi_2O_3$-CP catalyst was observed about 86.10 under UVC irradiation after 60 min reaction time and as can be clearly seen from the figure, the reaction rate gradually decreases under UVC irradiation; whereas under UVB irradiation after 60 min the photodegradation of PAR achieved 85.37% and completed degraded after 90 min reaction time. Photodegradation of PAR was investigated using $Bi_2O_3$-SG (1:2) catalyst by different light sources can be seen in Fig. 9(d), which clearly indicates that $Bi_2O_3$-SG (1:2) has the highest photocatalytic activity for PAR in this study. Almost all PAR (99.5%) was

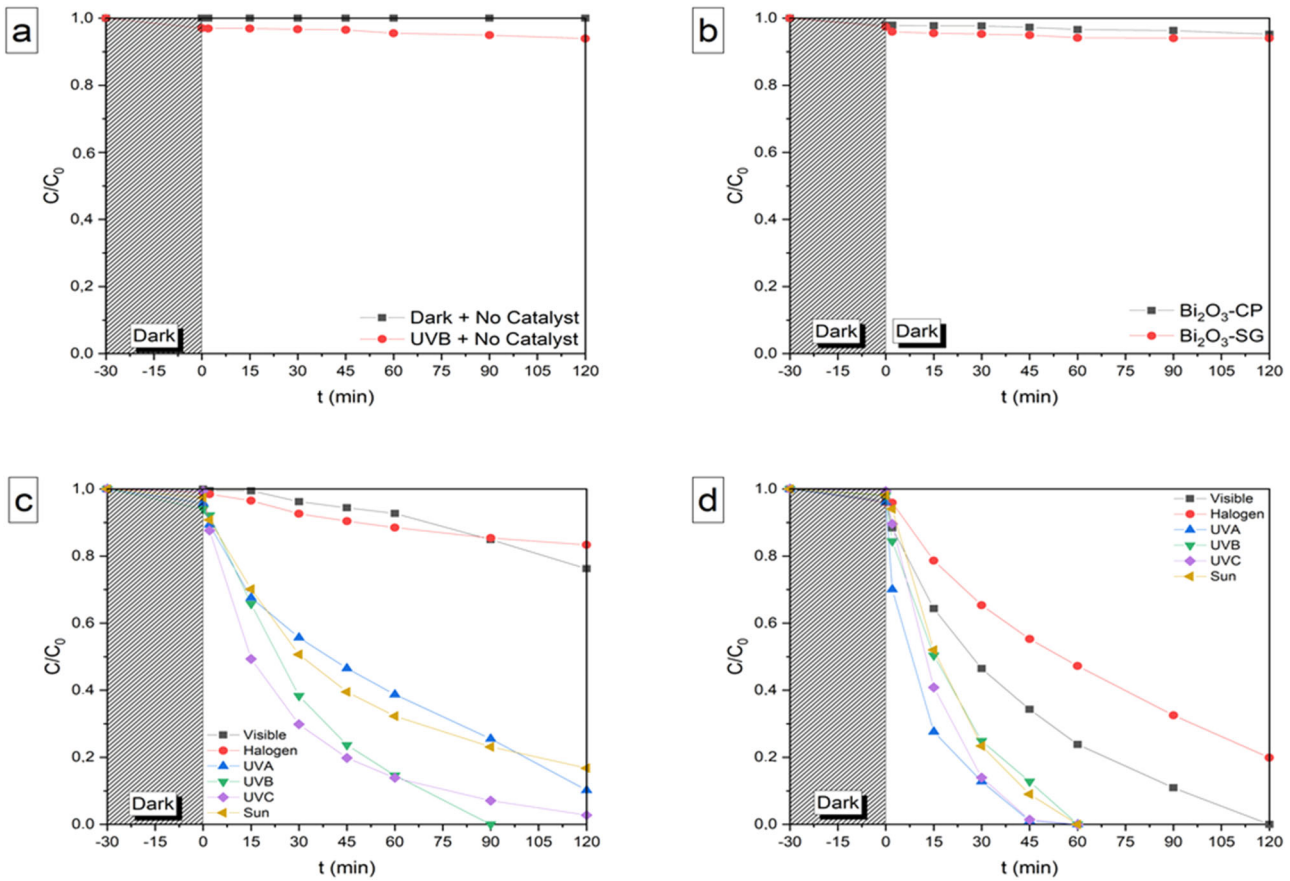



**Fig. 9** PAR degradation using **a** without any catalysts, **b** $Bi_2O_3$-CP and $Bi_2O_3$-SG catalysts under dark conditions **c** $Bi_2O_3$-CP, and **d** $Bi_2O_3$-SG under different light sources at pH 5

removed from the wastewater within 45 min reaction time by UVA, UVB and UVC light irradiation. In addition, PAR was completely removed after 60 min reaction time by UVA, UVB, UVC lights, and directly sunlight irradiation. It was determined that $Bi_2O_3$-SG (1:2) catalyst showed higher activities in a wider wavelength range. Thus, it can be seen that $Bi_2O_3$-SG (1:2) catalyst is significantly improved the photocatalytic degradation of PAR. It can be explained with the surface and optical properties of $Bi_2O_3$-SG (1:2). According to the characterization results, the decrease of band gap energy and crystallite size, and the increase of specific surface area were observed. Thus, it enhanced the photocatalytic activity.

### 3.2.3 Effect of initial pH

To investigate the influence of the initial pH level on PAR photodegradation a series of photocatalytic reactions were performed using $Bi_2O_3$–CP and $Bi_2O_3$-SG (1:2) catalysts under UVB and directly sun light irradiation at the wide pH range between 3–9, and the results were shown in Fig. 10. When the initial pH of PAR solution changed, the degradation efficiency changed. As can be seen from Fig. 10a, in the presence of the $Bi_2O_3$-CP, the photocatalytic degradation efficiency of PAR in the range between pH 5–9 increased with the decreased of the initial pH. At pH 5 condition, PAR completely removed from the wastewater within 90 min under UVB irradiation. However, it was observed that the photocatalytic degradation gradually decreased pH values below pH 5. In Fig. 10b, the photocatalytic degradation of PAR in the presence of $Bi_2O_3$-CP, under sunlight irradiation directly was investigated.

$Bi_2O_3$-SG (1:2) performed under both UV-B radiation and direct sunlight. In reactions, photocatalytic activity gradually decreases under reaction conditions above pH 5 has decreased. Below pH 5, the percentage of photocatalytic degradation first decreased and then increased. The highest photocatalytic activity obtained at pH 3. PAR was 100% degraded in 15 min under UV-B irradiation at pH 3 and decomposed 99.5% in 30 min under sunlight. The activities results are summarized in Table 2. As shown in Table 2, $Bi_2O_3$-SG (1:2) exhibits the highest $k$ value of 0.321 $min^{-1}$ than that of $Bi_2O_3$-CP catalyst. These $k$ values reveal the great photocatalytic efficiency of $Bi_2O_3$-SG (1:2). The high photocatalytic activity of $Bi_2O_3$-SG (1:2) photocatalyst is attributed to the porous morphology, higher surface area,

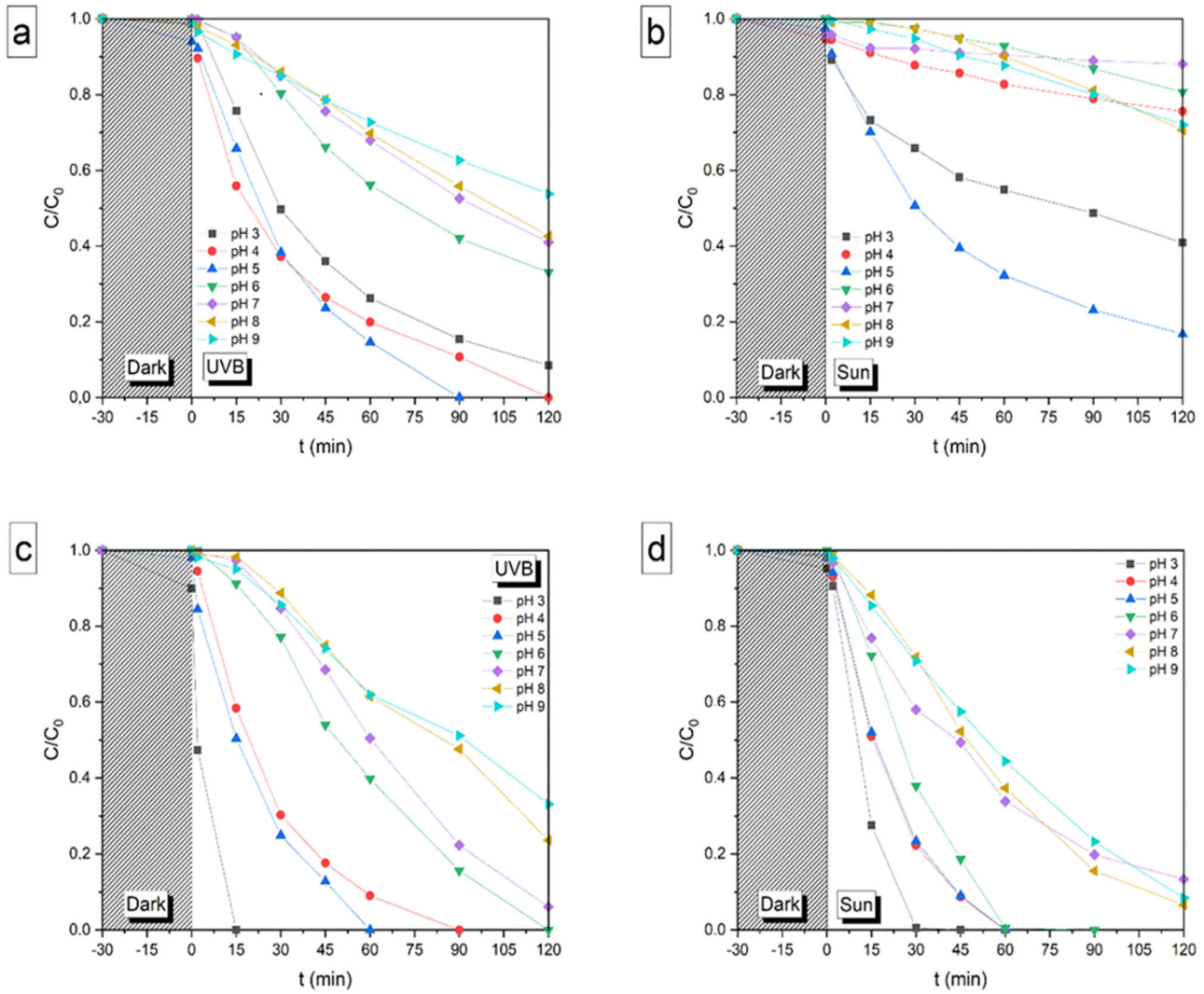



**Fig. 10** PAR degradation using (**a**, **b**) $Bi_2O_3$-CP and (**c**, **d**) $Bi_2O_3$-SG (1:2) photo-catalyst in the presence of UVB and directly sun, respectively

**Table 2** Degradation kinetics of PAR at pH 3 using $Bi_2O_3$-CP and $Bi_2O_3$-SG catalysts under different light sources

| Catalyst | Light Source | Rate Constant [k ($10^{-3}$ $min^{-1}$)] | Degradation (%) (at 15 min) | Regression Coefficient ($R^2$) |
|---|---|---|---|---|
| $Bi_2O_3$-CP | UV | 20.8 | 24.33 | 0.996 |
| | Sun | 10.5 | 26.77 | 0.965 |
| $Bi_2O_3$-SG | UV | 321 | 100 | 0.999 |
| | Sun | 85.7 | 72.4 | 0.985 |

and lower bad gap, which helps to achieve higher photo-catalytic performance.

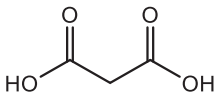
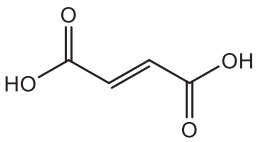
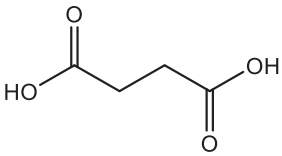
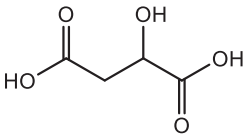
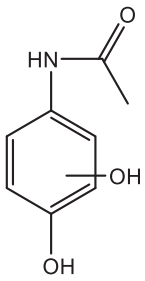
Exceptional situation at pH 3 LC-MS/MS of samples taken at different times to determine the cause analysis was carried out. The reactions occur via •OH attack on the aromatic ring of PAR. Due to the electrophilic attack of hydroxyl radicals, it is thought that it may cause the formation of different positional isomers (dihydroxyphenyl acetamide and monohydroxy paracetamol). As a result, such intermediates are repeatedly oxidation leads to the formation of malonic, malic, succinic, or fumaric (butenedionic) acid and thus it is suggested that it can be converted into more $CO_2$ and $H_2O$ [47, 48].

N-(dihydroxyphenyl) acetamide at the initial time ($t = 0$) at pH 5 for the $Bi_2O_3$-CP catalyst (monohydroxy paracetamol) was not found. Moreover, in the reaction that took place at pH 3 in the presence of $Bi_2O_3$-SG (1:2) catalyst, it has been understood that in addition to the conversion of PAR into carboxylic acids, possible isomers of N- (dihydroxyphenyl) acetamide (monohydroxy paracetamol) also transform into carboxylic acids by direct ring opening.

In a study, it was stated that PAR degraded by 83% after 150 min under UV irradiation at pH 9 with $TiO_2$ catalyst [49]. In addition, it was understood that 1% Pt-$TiO_2$ catalyst was completely degraded in 180 min under sunlight at pH 4.3 [50].

In addition, total organic carbon (TOC) analysis has been employed to detect the presence of organic intermediates

**Table 3** Identified intermediates during photocatalytic degradation of paracetamol

| Intermediates | Structure |
|---|---|
| Malonic acid |  |
| Fumaric acid (Butenedionic acid) |  |
| Succinic acid |  |
| Malic acid |  |
| Acetamide, N-(dihydroxyphenyl) |  |

and the photodegradation performance of catalysts with the photocatalytic degradation process. TOC removal results were evaluated on the photocatalytic degradation of PAR with $Bi_2O_3$-CP and $Bi_2O_3$-SG (1:2) at pH 5 under UV-B irradiation. 99.19% TOC removal can be achieved in 60 min with $Bi_2O_3$-SG (1:2). This result emphasizes the achievement of the total mineralization. However, the TOC removal reached to 88.97% with $Bi_2O_3$-CP, which can not completely degraded in 60 min. As a result, the completely mineralization of pharmaceutical substances such as paracetamol into simple molecules that are harmless to the environment by photocatalytic degradation method has been achieved with a $Bi_2O_3$-SG (1:2) catalyst.

### 3.3 Hydroxyl radical formation

$Bi_2O_3$ does strongly absorb ultraviolet (UV) radiation (*hv*), leading to the formation of hydroxyl radicals. Assumed reaction mechanisms of photocatalytic processes of paracetamol via $Bi_2O_3$ as below [51]:

$$Bi_2O_3 + h\nu \rightarrow e^-_{cb} + h^+_{\nu b}$$

$$h^+_{\nu b} + H_2O \rightarrow \bullet OH + H^+$$

$$h^+_{\nu b} + OH^- \rightarrow \bullet OH$$

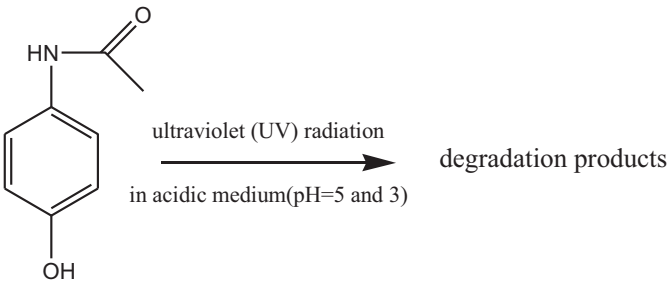
$$\text{Organics} + h^+_{\nu b} \rightarrow \text{degradation products}$$

$$e^-_{cb} + O_2 \rightarrow O_2^{\bullet -},$$

$$\text{Organics} + e^-_{cb} \rightarrow \text{degradation products}$$

Produced hydroxyl radicals (•OH) along with other oxidants, such as the superoxide radical anion ($O_2^{\bullet -}$), can further mineralize organic compounds to end products (water and $CO_2$).

$$\text{Organics} + (\bullet OH, O_2^{\bullet -}, \text{etc.}) \rightarrow \text{degradation products}$$



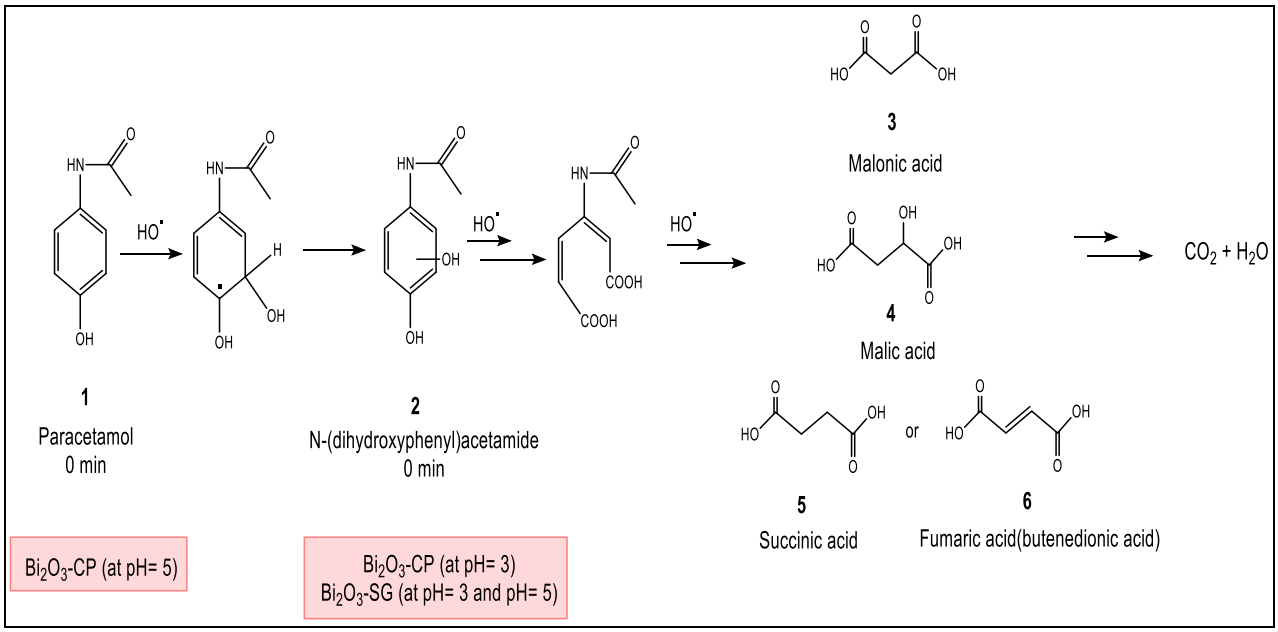

The identified intermediates during photocatalytic degradation of paracetamol were given in Table 3.

### 3.4 The reaction mechanism

From their chemical structures determined by LC-MS/MS analysis, a reaction pathway for the degradation of paracetamol solution under UV irradiation with $Bi_2O_3$ photocatalyst was proposed (Scheme 1).

It is well known that the degradation of organic compounds by the $Bi_2O_3$/UV system occurs through the in situ production of free hydroxyl radicals (•OH). This reaction is proposed to occur by the Bi2O3 photocatalyst through an initial UV-light absorption at wavelengths higher than the band gap, sufficient to form the so-called electron-hole (h+/e−) pair. The excited electron can reduce the oxygen molecule to form the radical anion $O_2$, whereas the hole $h^+$ can react either with the target compound or with water, leading to the formation of hydroxyl radicals (•OH), extremely reactive species.

They can easily attack organic molecules and thus initiate a series of reactions with partial or complete degradation




**Scheme 1** Total mechanism of PAR oxidation by UV/$Bi_2O_3$ [52]

of target organic compounds [52]. In Scheme 1, an initial •OH attack on the aromatic ring of paracetamol (1) is proposed. This attack can result in the formation of: (i) two positional isomers of N-(dihydroxyphenyl)acetamide (monohydroxyparacetamol) (2) through electrophilic attack of the hydroxyl radical at both available positions of the aromatic ring of paracetamol. 1). Finally, sequential oxidation of such an intermediate is suggested to lead to the formation of malonic (3), malic (4), succinic (5), or fumaric (butenedionic) (6) acid; This acid can then be converted (in) into $CO_2$ and $H_2O$ (in a process known as mineralization). Products are very similar and also described here [47, 48].

In addition, experiments showed that for $Bi_2O_3$-CP catalyst (at pH = 5), monohydroxy PAR could not be detected initially ($t = 0$ min); degradation occurred via PAR. With the use of $Bi_2O_3$-CP (at pH = 3) and $Bi_2O_3$-SG (1:2) (both of pH = 3 and 5), monohydroxy paracetamol was detected firstly. Decomposition occurred through this intermediate.

### 3.5 Future prospects

In order to achieve the expected goal in a photocatalytic process, it is important to produce photocatalysts at a lower cost, as well as features such as easy production, reuse, stability, optimum performance and activity in visible light source. The synthesized $Bi_2O_3$-SG material can be used in various photocatalytic applications (degradation of pollutants in water and air, water splitting, reduction of $CO_2$ and organic synthesis) has taken its place among other bismuth-based catalysts as a successful photocatalyst. It is hoped that resistant chemical substances such as paracetamol will be degraded in a very short time in UV/sunlight, and that improvements will be made in some other applications such as cancer treatment and antibiotic use.

However, it is noteworthy that there is still work to be done to design, synthesize and apply these materials. Though there are bismuth-based materials and their applications in the literature, these materials still have properties that need to be improved. Bismuth-based composite materials can be synthesized at lower tempetrature and the surface properties of them can be developed to have high surface area for achieving enhanced photocatlytic activity.

In reaction applications, photocatalytic activity can be increased by designing reactors with different features/types and sizes. In addition to the research in the literature, optimization at higher pollutant concentrations constitutes an important scope in targeted studies. It is important to develop photosensitive materials to perform under visible light. In addition, there is a need to both produce and process materials that have shown high activity in laboratory-scale applications in the large scale.

## 4 Conclusions

In this research, $Bi_2O_3$ nanostructures were successfully prepared by co-precipitation and sol–gel method. The sol–gel synthesis significantly improved the photocatalytic activities and decreased particle size, band gap energy, and PL intensity. The operation conditions in terms of molar ratio of bismuth acetate to oxalic acid, pH, and the source of light irradiation were optimized for PAR photodegradation

studies. The optimal ratio of bismuth acetate to oxalic acid was found as 1:2. Besides, the initial pH of PAR solution affected the photocatalytic degradation performance. $Bi_2O_3$-SG (1:2) exhibited enhanced activity at pH 3 value under UVB light source. The highest removal of PAR is 100% within 15 min under UVB irradiation which follows the pseudo-first order kinetics with the rate constant is 0.321 $min^{-1}$ and decomposed 99.5% in 30 min under sunlight.

The chemical structures of the compounds detected by the LC–MS/MS analysis. The experiments proved using $Bi_2O_3$-CP (at pH = 3), and $Bi_2O_3$-SG (1:2) (both of pH = 3 and 5), monohydroxy paracetamol was detected firstly. In conclusion, the photocatalytic application of $Bi_2O_3$-SG (1:2) sunlight/UVB light is an efficient technique for the degradation and mineralization of hazardous and persistent pharmaceutical contaminants. Further research can be conducted on optimizing the sol–gel process for broader commercial applicability.

## Data availability

No datasets were generated or analysed during the current study.

**Acknowledgements** The authors would like to sincerely express their thanks to the Scientific Research Projects (BAP) Coordination Unit of Istanbul University-Cerrahpaşa for supporting the project under project no.: 33505.

**Author contributions** Conceptualization: Gulin Selda Pozan Soylu; Methodology: Gulin Selda Pozan Soylu, Derman Akşit; Formal analysis and investigation: Derman Aksit, Cigdem Sayil; Writing—original draft preparation: Derman Aksit, Gulin Selda Pozan Soylu; Writing—review and editing: Gulin Selda Pozan Soylu, Derman Aksit, CigdemSayil; Resources: Derman Aksit, Gulin Selda Pozan Soylu; Supervision: Gulin Selda Pozan Soylu.

**Funding** This study was supported by the research project number FBA-2020-33505 of the Scientific Research Projects Coordination Unit of İstanbul University-Cerrahpaşa. Open access funding provided by the Scientific and Technological Research Council of Türkiye (TÜBİTAK).

## Compliance with ethical standards

**Conflict of interest** The authors declare no competing interests.

**Publisher's note** Springer Nature remains neutral with regard to jurisdictional claims in published maps and institutional affiliations.

**Open Access** This article is licensed under a Creative Commons Attribution 4.0 International License, which permits use, sharing, adaptation, distribution and reproduction in any medium or format, as long as you give appropriate credit to the original author(s) and the source, provide a link to the Creative Commons licence, and indicate if changes were made. The images or other third party material in this article are included in the article's Creative Commons licence, unless indicated otherwise in a credit line to the material. If material is not included in the article's Creative Commons licence and your intended use is not permitted by statutory regulation or exceeds the permitted use, you will need to obtain permission directly from the copyright holder. To view a copy of this licence, visit http://creativecommons.org/licenses/by/4.0/.

## References

1. Oturan MA, Aaron JJ (2014) Advanced oxidation processes in water/wastewater treatment: principles and applications. a review. Critical Reviews in Environ Sci Technol 44(23):2577–2641. https://doi.org/10.1080/10643389.2013.829765.
2. Swaminathan M, Muruganandham M, Sillanpaa M (2019) Advanced oxidation processes for wastewater treatment. Inter J Photoenergy. https://doi.org/10.1155/2013/683682.
3. Vaiano V, Sacco O, Sannino D, Ciambelli P (2015) Photocatalytic removal of spiramycin from wastewater under visible light with N-doped $TiO_2$ photocatalysts. Chem Eng J 261:3–8. https://doi.org/10.1016/j.cej.2014.02.071.
4. Liang Q, Liu X, Zeng G et al. (2019) Surfactant-assisted synthesis of photocatalysts: mechanism, synthesis, recent advances and environmental application. Chem Eng J 372:429–451. https://doi.org/10.1016/j.cej.2019.04.168.
5. Tang L, Wang J, Zeng G et al. (2016) Enhanced photocatalytic degradation of norfloxacin in aqueous bi2wo6 dispersions containing nonionic surfactant under visible light irradiation. J Hazard Mater 306:295–304. https://doi.org/10.1016/j.jhazmat.2015.12.044.
6. Wu S, Zhang L, Chen J (2012) Paracetamol in the environment and its degradation by microorganisms. Appl Microbiol Biotechnol 96(4):875–884. https://doi.org/10.1007/s00253-012-4414-4.
7. Yang L, Yu LE, Ray MB (2009) Photocatalytic oxidation of paracetamol: dominant reactants, intermediates, and reaction mechanisms. Environ Sci Technol 43(2):460–465. https://doi.org/10.1021/es8020099.
8. Yang L, Yu LE, Ray MB (2008) Degradation of paracetamol in aqueous solutions by $TiO_2$ photocatalysis. Water Research 42(13):3480–3488. https://doi.org/10.1016/j.watres.2008.04.023.
9. Bedner M, MacCrehan WA (2006) Transformation of acetaminophen by chlorination produces the toxicants 1,4-benzoquinone and n-acetyl-p-benzoquinone imine. Environ Sci Technol 40(2):516–522. https://doi.org/10.1021/es0509073.
10. Aziz FFA, Jalil AA, Triwahyono S, Mohamed M (2018) Controllable structure of fibrous $SiO_2$–ZSM-5 support decorated with $TiO_2$ catalysts for enhanced photodegradation of paracetamol. Appl Surf Sci 455:84–95. https://doi.org/10.1016/j.apsusc.2018.05.183.
11. Lin C-J, Yang W-T (2014) Ordered mesostructured Cu-doped $TiO_2$ spheres as active visible-light-driven photocatalysts for degradation of paracetamol. Chem Eng J 237:131–137. https://doi.org/10.1016/j.cej.2013.10.027.
12. Saeed AM (2017) Spectrophotometric determination of paracetamol in some manufactured tablets in Iraqi markets. Int J Pharm Sci Rev Res 42(2):53–57.
13. Jiang H-Y, Liu J, Cheng K, Sun W, Lin J (2013) Enhanced visible light photocatalysis of $Bi_2O_3$ upon fluorination. J Phys Chem C 117(39):20029–20036. https://doi.org/10.1021/jp406834d.
14. Gao P, Yang Y, Yin Z, Kang F, Fan W et al. (2021) A critical review on bismuth oxyhalide based photocatalysis for pharmaceutical active compounds degradation: modifications, reactive sites, and challenges. J Hazard Mater 412:125186. https://doi.org/10.1016/j.jhazmat.2021.125186.

15. Arthur R, Ahern J, Patterson H (2018) Application of BiOX photocatalysts in remediation of persistent organic pollutants. Catalysts 8(12):604–628. https://doi.org/10.3390/catal8120604.
16. Hussain A, Hou J, Tahir M, Ali SS et al. (2022) Recent advances in BiOX-based photocatalysts to enhanced efficiency for energy and environment applications. Catal Rev 8:1–55. https://doi.org/10.1080/01614940.2022.2041836.
17. Chen X, Chen P, Yang S, Gao H (2022) Recent advances in bismuth oxyhalides photocatalysts and their applications. Nanotechnology 34(5):052001. https://doi.org/10.1088/1361-6528/aca02e.
18. Mirzaei A, Chen Z, Haghighat F, Yerushalmi L (2016) Removal of pharmaceuticals and endocrine disrupting compounds from water by zinc oxide-based photocatalytic degradation: A review. Sustainable Cities and Society 27:407–418.
19. Lum PT, Foo KY, Zakaria NA (2019) Visible light driven photocatalytic degradation of paracetamol using incense ash supported ZnO nanocomposites. Malaysian J Anal Sci 23(5):771–780. https://doi.org/10.17576/mjas-2019-2305-02.
20. Shakir M, Faraz M, Sherwani MA, Al-Resayes SI (2016) Photocatalytic degradation of the Paracetamol drug using Lanthanum doped ZnO nanoparticles and their in-vitro cytotoxicity assay. J Lumin 176:159–167. https://doi.org/10.1016/j.jlumin.2016.03.027.
21. Basha S, Keane D, Nolan K, Oelgemöller M, Lawler J, Tobin JM, Morrissey A (2015) UV-induced photocatalytic degradation of aqueous acetaminophen: the role of adsorption and reaction kinetics. Environ Sci Pollut Res 22:2219–2230. https://doi.org/10.1007/s11356-014-3411-9.
22. Lin JC-T, de Luna MDG, Gotostos MJN, Lu M-C (2015) Optimization of visible-light photocatalytic degradation of acetaminophen by K3[Fe(CN)6]-modified $TiO_2$. J Taiwan Inst Chem Eng 49:129–135. https://doi.org/10.1016/j.jtice.2014.11.030.
23. Khairnar SD, Shrivastava VS (2019) Photocatalytic degradation of chlorpyrifos and methylene blue using α-$Bi_2O_3$ nanoparticles fabricated by sol–gel method. SN Appl Sci 1(7):762. https://doi.org/10.1007/s42452-019-0761-4.
24. Fajrina N, Tahir M (2019) A critical review in strategies to improve photocatalytic water splitting towards hydrogen production. Int J Hydrogen Energy 44(2):540–577. https://doi.org/10.1016/j.ijhydene.2018.10.200.
25. Devika S, Rajesh J, Tayade (2022) Low temperature energy-efficient synthesis methods for bismuth-based nanostructured photocatalysts for environmental remediation application: a review. Chemosphere 304:135300. https://doi.org/10.1016/j.chemosphere.2022.135300.
26. Natarajan TS, Natarajan K, Bajaj HC, Tayade RJ (2013) Enhanced photocatalytic activity of bismuth-doped TiO2 nanotubes under direct sunlight irradiation for degradation of Rhodamine B dye. J Nanopart Res 15:1669. https://doi.org/10.1007/s11051-013-1669-3.
27. Meroni D, Pifferi V, Sironi B, Cappelletti G, Falciola L, Cerrato G, Ardizzon S (2012) Block copolymers for the synthesis of pure and Bi-promoted nano-$TiO_2$ as active photocatalysts. J Nanopart Res 14:1086. https://doi.org/10.1007/s11051-012-1086-z.
28. Natarajan K, Bajaj HC, Tayade RJ (2016) Photocatalytic efficiency of bismuth oxyhalide (Br, Cl and I) nanoplates for RhB dye degradation under LED irradiation. J Indust Eng Chem 34:146–156. https://doi.org/10.1016/j.jiec.2015.11.003.
29. Dong S, Liu X, Tian G, Wang Y, Jin G, Zhao Y, Sun J, Fan M (2022) Surface oxygen vacancies modified $Bi_2MoO_6$ double-layer spheres: Enhanced visible LED light photocatalytic activity for ciprofloxacin degradation. J Alloy Compd 892:162217. https://doi.org/10.1016/j.jallcom.2021.162217.
30. Liu Z, Tai Y, Liu J, Liu F, Han B, Fu W, Yang X, Xie H, Liu Q (2022) A novel mechanism for visible-light degradation of phenol by oxygen vacancy $Bi_2MoO_6$ homojunction. Appl Surf Sci 605:154671. https://doi.org/10.1016/j.apsusc.2022.154671.
31. Mustapha S, Tijani JO, Ndamitso MM, Abdulkareem AS, Shuaib DT, Amigun AT, Abubakar HL (2021) Facile synthesis and characterization of $TiO_2$ nanoparticles: X-ray peak profile analysis using Williamson–Hall and Debye–Scherrer methods. Int Nano Lett 11(3):241–261. https://doi.org/10.1007/s40089-021-00338-w.
32. Cao L, Spiess FJ, Huang A, Suib SL, Obee TN et al. (1999) Heterogeneous photocatalytic oxidation of 1-Butene on $SnO_2$ and $TiO_2$ films. J Phys Chem B 103(15):2912–2917. https://doi.org/10.1021/jp983860z.
33. Zhang L, Wang W, Yang J, Chen Z, Zhang W et al. (2006) Sonochemical synthesis of nanocrystallite $Bi_2O_3$ as a visible-light-driven photocatalyst. Appl Catal A: Gen 308:105–110. https://doi.org/10.1016/j.apcata.2006.04.016.
34. Iyyapushpam S, Nishanthi ST, Pathinettam Padiyan D (2014) Enhanced photocatalytic degradation of methyl orange by gamma $Bi_2O_3$ and its kinetics. J Alloys Comp 601:85–87. https://doi.org/10.1016/j.jallcom.2014.02.142.
35. Makuła P, Pacia M, Macyk W (2018) How to correctly determine the band gap energy of modified semiconductor photocatalysts based on UV–Vis spectra. J Phys Chem. Lett 9(23):6814–6817. https://doi.org/10.1021/acs.jpclett.8b02892.
36. Sasca V, Popa A (2013) Band-gap energy of heteropoly compounds containing keggin polyanion-[PVxMo12-XO40]−(3+x) relates to counter-cations and temperature studied by UV-VIS diffuse reflectance spectroscopy. J Appl Phys 14(13):133503. https://doi.org/10.1063/1.4820582.
37. Eberl J, Kisch H (2008) Visible light photo-oxidations in the presence of α-$Bi_2O_3$. Photochem Photobiol Sci 7:1400–1406.
38. Carlsson JM, Hellsing B, Domingos HS, Bristowe PD(2002) Theoretical investigation of the pure and Zn-doped 훼 and 훿 phases of $Bi_2O_3$ Phys. Rev. B 65:205122. https://doi.org/10.1103/PhysRevB.65.205122.
39. Abu-Dief AM, Mohamed WS (2017) α-$Bi_2O_3$ nanorods synthesis, characterization and UV-photocatalytic activity. Mater Res Express 4(3):035039. https://doi.org/10.1088/2053-1591/aa6712.
40. Abdullahi SS, Güner S, Koseoglu Y, Musa İM, Adamu BI, Abdulhamid MI (2016) Sımple method for the determination of band gap of a nanopowdered sample usıng Kubelka Munk theory. J NAMP 35:241–246.
41. Hao Q, Liu Y, Chen T, Guo Q, Wei W, Ni B-J (2019) $Bi_2O_3$@Carbon nanocomposites for solar-driven photocatalytic degradation of chlorophenols. ACS Appl Nano Mater 2(4):2308–2316. https://doi.org/10.1021/acsanm.9b00206.
42. Majhi D, Samal PK, Das K, Gouda SK, Bhoi YP, Mishra BG (2019) α-NiS/Bi2O3 nanocomposites for enhanced photocatalytic degradation of tramadol. ACS Appl Nano Mater 2(1):395–407. https://doi.org/10.1021/acsanm.8b01974.
43. Gandhi AC, Lai C-Y, Wu K-T, Ramacharyulu PVRK, Koli VB, Cheng C-L, Ke S-C, Wu SY (2020) Phase transformation and room temperature stabilization of various Bi2O3 nano-polymorphs: effect of oxygen-vacancy defects and reduced surface energy due to adsorbed carbon species. Nanoscale 12(47):24119–24137. https://doi.org/10.1039/D0NR06552H.
44. Gandhi AC, Cheng CL, Wu SY (2020) Structural and enhanced optical properties of stabilized Γ–$Bi_2O_3$ nanoparticles: effect of oxygen ion vacancies. Nanomaterials 10(6):1023. https://doi.org/10.3390/nano10061023.
45. Luciano AJR, de Sousa Soletti, Ferreira MEC, Cusioli LF, de Andrade MB, Bergamasco R, Yamaguchi NU (2020) Manganese ferrite dispersed over graphene sand composite for methylene blue photocatalytic degradation. J Environ Chem Eng 8(5):104191. https://doi.org/10.1016/j.jece.2020.104191.
46. Yamaguchi NU, Bergamasco R, Hamoudi S (2016) Magnetic $MnFe_2O_4$–graphene hybrid composite for efficient removal of

glyphosate from water. Chem Eng J 295:391–402. https://doi.org/10.1016/j.cej.2016.03.051.
47. Vogna D, Marotta R, Napolitano A, d'Ischia M (2002) Advanced oxidation chemistry of Paracetamol. UV/$H_2O_2$-induced hydroxylation/degradation pathways and 15N-aided inventory of nitrogenous breakdown products. J Org Chem 67(17):6143–6151. https://doi.org/10.1021/jo025604v.
48. Andreozzi R, Caprio V, Marotta R, Vogna D (2003) Paracetamol oxidation from aqueous solutions by means of ozonation and $H_2O_2$/UV system. Water Research 37(5):993–1004. https://doi.org/10.1016/S0043-1354(02)00460-8.
49. Jallouli N, Elghniji K, Trabelsi H, Ksibi M (2017) Photocatalytic degradation of paracetamol on $TiO_2$ nanoparticles and $TiO_2$/cellulosic fiber under UV and sunlight irradiation. Arabian J Chem. https://doi.org/10.1016/j.arabjc.2014.03.014.
50. Nasr O, Mohamed O, Al-Shirbini A-S, Abdel-Wahab A-M (2019) Photocatalytic degradation of acetaminophen over Ag, Au and Pt loaded $TiO_2$ using solar light. J Photochem Photobiology A Chem 374:185–193. https://doi.org/10.1016/j.jphotochem.2019.01.032.
51. Abhinay S, Mazumder RA (2021) Novel 0.9$KNbO_3$–0.1BaNi0.5Nb0.5$O_3$(KBNNO): $Ag_2O/Bi_2O_3$ heterojunction photocatalyst: synthesis, characterization and excellent photocatalytic performance. J Mater Sci Mater Electron 32(13):17061–17077. https://doi.org/10.1007/s10854-021-05982-8.
52. Dalmázio I, Alves TMA, Augusti R (2008) An appraisal on the degradation of paracetamol by $TiO_2$/UV system in aqueous medium: product identification by gas chromatography-mass spectrometry (GC-MS). J Braz Chem Soc 19:81–88. https://doi.org/10.1590/S0103-50532008000100013.